Available online at www.sciencedirect.com
ScienceDirect
Tetrahedron 64 (2008) 1301–1308
Tetrahedron
www.elsevier.com/locate/tet

Self-assembled helical ribbon and tubes of alanine-based amphiphiles induced by two different formation mechanisms

Soo Jin Lee [a], Eunjeong Kim [a], Moo Lyong Seo [a], Youngkyu Do [b], Young-A Lee [c], Shim Sung Lee [a], Jong Hwa Jung [a,*], Masaki Kogiso [d,e], Toshimi Shimizu [d,e,*]

[a] *Department of Chemistry, Research Institute of Natural Science, Gyeongsang National University, 900 Gazwa-dong, Jinju 660-701, Republic of Korea*
[b] *Department of Chemistry, Korea Advanced Institute of Science and Technology (KAIST), Daejeon 305-701, Republic of Korea*
[c] *Department of Chemistry, Chonbuk National University, Jeonju 561-756, Republic of Korea*
[d] *SORST, Japan Science and Technology Agency, Tsukuba Central 5, 1-1-1 Higashi, Tsukuba, Ibaraki 305-8565, Japan*
[e] *Nanoarchitectonics Research Center, National Institute of Advance Industrial Science and Technology, Tsukuba Central 5, 1-1-1 Higashi, Tsukuba, Ibaraki 305-8565, Japan*

Received 21 September 2007; received in revised form 19 November 2007; accepted 20 November 2007
Available online 22 November 2007

Abstract

Three long chain alanine-based amphiphiles (**1**–**3**) possessing either a saturated long alkyl chain group or unsaturated groups as the self-assembling unit of a highly organized molecular architecture were synthesized. Their self-assembling properties were investigated using EF-TEM, SEM, CD, XRD, and FTIR. The D-form (**1**) and the L-form (**2**) enantiomers showed the opposite CD signals. Furthermore, electron micrographs of the self-assembled **1** and **2** exhibited right- and left-handed helical structures, respectively. The helical structures of amphiphiles **1** and **2** were developed into tubular structures by slow cooling. On the other hand, in the helical ribbon growth process, the helical pitch and ribbon width were changed in fast cooling process. The findings strongly imply that the helical ribbon growth of alanine-based amphiphiles can be induced by two different pathways. This mechanism, quite different from that observed for sugar- and cholesterol-based tubes, is a rare example for a tube formation process.

Keywords: Alanines; Amphiphiles; Helical ribbons; Self-assembly

1. Introduction

The importance of chirality, or molecular handedness, has long been recognized in many areas of chemistry and physics. The interactions between chiral molecules change dramatically when one molecule is replaced by its corresponding mirror image structure. The advantage of chiral specificity has been recognized by the pharmaceutical industry and is the basis of a major effort to synthesize chiral drugs.[1] Likewise, in the area of liquid crystals, molecular chirality leads to the formation of phases with long-range helical modulations, such as the cholesteric phase.[2]

Helical ribbon growth occurs by two different routes. It arise from exclusive consequence happenings, which are the shortening of the helical pitch of the ribbon and the increase in the tape width. Thus, one occurs with the former while the latter does not change and vice versa for the other. For example, sugar-based amphiphiles[3,4] produced tubular structures by the former process whereas cholesterol-based amphiphiles induced tubule formation by the latter one.[3,5] However, cases of helical ribbon growth by widening of the tape with no concomitant change in helical pitch (second route) are more common in the literature than the former route. In almost all cases, the importance of pitch or width changes in self-assembled amphiphiles is not clear in the helical ribbon growth mechanism.

Helical ribbon structures in various systems of chiral organic molecules, including diacetylenic lipids, surfactant, bile, and

* Corresponding authors. Tel.: +82 55 751 6027; fax: +82 55 758 6027.
E-mail address: jonghwa@gnu.ac.kr (J.H. Jung).

0040-4020/$ - see front matter © 2007 Elsevier Ltd. All rights reserved.
doi:10.1016/j.tet.2007.11.062

glutamates, were grown into tubules.[6] In particular, the fabrication of tubular structures in phospho- and sugar-based lipids has been investigated by the introduction of diacetylenic groups.[7] However, the importance of diacetylenic units in the formation of other tubular structures has not been studied. Only a few examples of the mechanism of growth of tubules have appeared in the literature.[8] For examples, Kunitake and co-workers[9] found that certain amphiphiles can form tubular structures by way of a helical ribbon structure in aqueous solution, with growth of the tubular structure occurring by an increase of the width of the helical ribbon.

It is very well known that the various constituent molecules play very important role in the formation of the helical ribbon and tubular structures.[3,6,8–10] Currently, most of the research on the self-assembly of peptide amphiphiles were focused on the preparation and physical properties of self-assembled nanofibers, helical ribbon, and tubular structures.[11–13] However, the mechanism of growth of these helical ribbon structures derived from peptide-based amphiphiles was not conducted in any them.[9a,14] In this study, the growing mechanism and morphological control of the self-assembled peptide amphiphiles were investigated.

With these objectives in mind, we have newly synthesized a stereochemical series of alanine-based amphiphiles **1** and **2** as shown in Figure 1 and Scheme 1. Compound **3**, in the absence of diacetylene units, was synthesized as a reference compound to confirm the critical roles for the hydrophobic interactions between alkyl chain groups in the self-assembly formation. We herein report on the morphological control and the self-assembly behaviors of the self-assembled **1** and **2**, respectively. We also provide clear evidence regarding the growth mechanism of the helical ribbon structure of peptide-based amphiphiles by two different mechanisms. This is the first study that examines the effect of the introduction of diacetylenic units on tubule growth that ultimately leads to the formation of the diacetylenic peptide-based amphiphiles. The self-assembled morphologies were strongly dependent on the stereochemical enantiomer and unsaturated bonds in the lipophilic region. Furthermore, on the basis of circular dichroism and powder X-ray diffraction experiments, we provide evidence for the chiral packing structures of self-assembling superstructures of alanine-based amphiphiles.

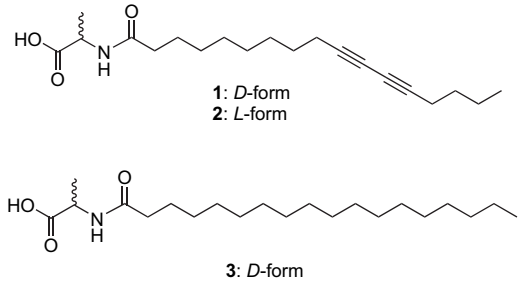

Figure 1. Chemical structures of **1**–**3**.

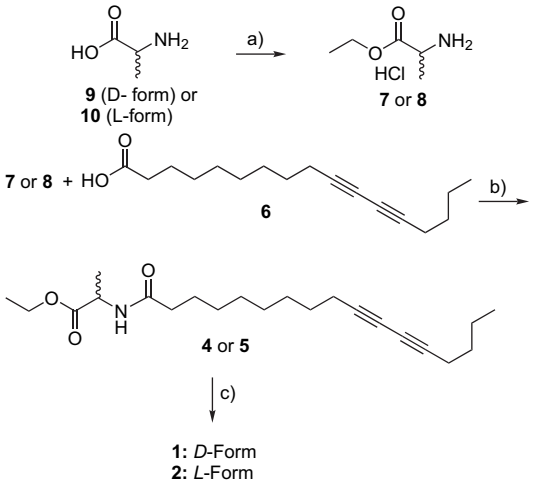

Scheme 1. Synthetic routes for amphiphiles **1** and **2**. (a) $SOCl_2$, EtOH, 86%; (b) DCC, HOBt, EA, 95%; (c) NaOH, MeOH, H_2O, 95%. DCC=1,3-dicyclohexylcarbodiimide, HOBt=1-hydroxybenzotriazole, EA=ethyl acetate.

2. Results and discussion

2.1. Synthesis of alanine-based amphiphiles

Two enantiomer alanine-based amphiphiles **1** and **2** were synthesized as shown in Scheme 1. Coupling of **7** with 10,12-heptadecadiynoic acid **6** provides **4** in 70% yield. Similar reaction gives **5** with 75% yield. Then, treatment of **4** or **5** with NaOH gave desired **1** and **2** in 95 and 92% yield, respectively. The products were purified using silica gel column chromatography. Also, compound **3** possessing saturated long alkyl chain group instead of the diacetylene unit was prepared as a reference by similar methods to confirm the role of the diacetylene unit (Supplementary data: Scheme S1).

2.2. Self-assembly and morphological observations

The self-assembled nanostructures of amphiphiles **1**–**3** were fabricated by two different methods as follows. Each alanine-based amphiphiles (1.0 mg) was dispersed into water (10.0 mL) at temperatures above the corresponding melting point (T_m) of the hydrated sample. In general, heating the mixture at 95 °C for 30 min was sufficient to obtain a homogeneous transparent solution. During the heating process, the sample flasks were wrapped with Al foil to prevent the polymerization.

The aqueous solutions were allowed to cool to room temperature at two different rates, 5.0 and 0.5 °C/min. Then, we observed and compared the morphologies of the self-assemblies prepared with fast and slow cooling rates at same aging step.

To precisely characterize the resultant morphologies and their size dimensions, we observed the individual self-assembled structures using energy-filtering transmission electron microscopy (EF-TEM) and scanning electron microscopy (SEM). In SEM and EF-TEM images of the self-assembled **1** prepared by cooling at 5.0 °C/min in aqueous solution exhibited a right-handed helical ribbon structure with a width of 4–10 μm and 24 μm of helical pitch (Fig. 2a), with all the

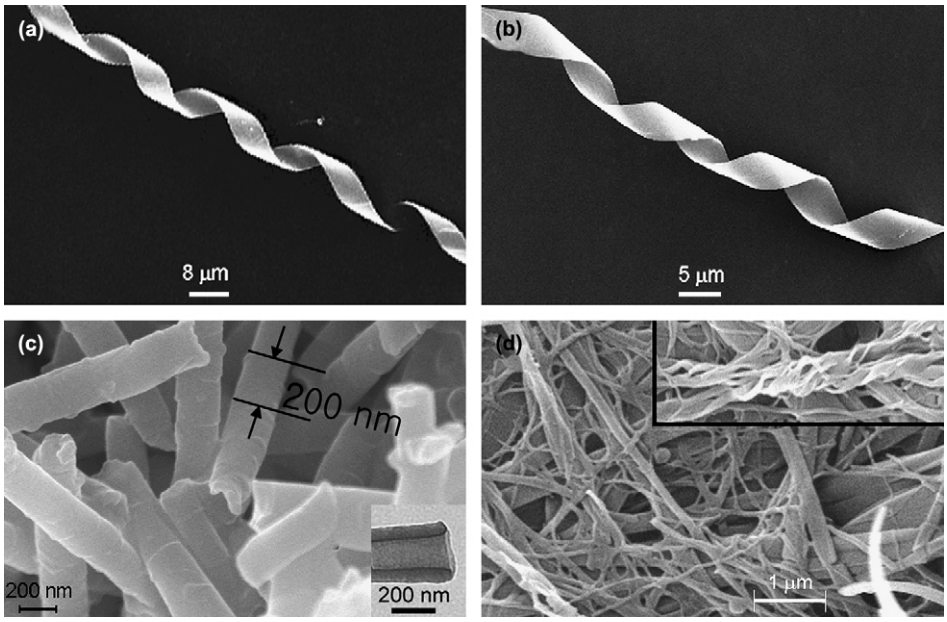

Figure 2. SEM images of self-assembled (a) **1** and (b) **2** prepared by fast cooling with 5.0 °C/min. SEM images of self-assembled (c) **1** prepared by slow cooling with 0.5 °C/min [inset, TEM image]. (d) SEM image of the self-assembled **3** prepared by fast cooling.

helicity possessing the right-handed helical motif. The self-assembled **2**, in contrast, exhibited all left-handed helical ribbon structure, 5–10 μm wide and with an 18 μm helical pitch (Fig. 2b). These results indicate that the helicity of self-assembled nanostructures is strongly influenced by the stereoisomeric alanine unit.

On the other hand, when self-assembled **1** was prepared by slow cooling at a rate of 0.5 °C/min, a helical ribbon morphology occurred, with an outer diameter of the intermediate morphological construction equal to 260 nm and the morphology of the final nanotubular structure exhibiting an inner diameter of ca. 120 nm and a wall thickness of 70 nm (Fig. 2c). Therefore, the cooling rate is an important factor in the production of nanotubes through self-assembly. The helical pitch for the tubular structure of self-assembled **1** prepared by slow cooling has almost same value, indicating that the growth mechanism for the self-assembled tubes **1** in slow cooling process is different from that in fast cooling. Also, the similar result was observed for the self-assembled **2** (Supplementary data: Fig. S1).

To confirm the diacetylene unit effect in the formation of helical structures, we introduced the saturated alkyl chain group into the lipophilic region of **3** instead of diacetylene unit of **1**. The self-assembled **3** exhibits the linear and the loosely helical structures with 50–200 nm of width (Fig. 2d), further supporting the view that the morphology formation of the alanine-based amphiphile depends strongly on the nature of the diacetylene unit in the long alkyl chain group.

Photopolymerization of the self-assembled **1** and **2** by irradiation at 254 nm wavelength with 6 W UV lamp at a distance of 10 cm for 30 min results in a red solution with an absorption maximum at 575 nm (Fig. 3). During irradiation process, the self-assembled samples were maintained at 10 °C to prevent the undesired side reaction. The color change from

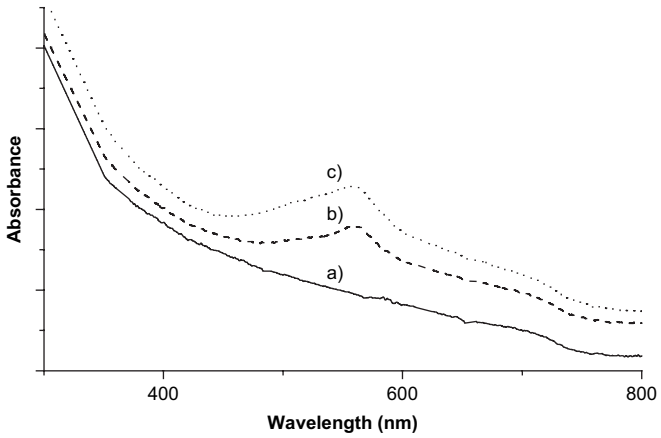

Figure 3. Solid UV–vis absorption spectra for self-assembled **1** (a) before and (b) after irradiation for 15 min and (d) 30 min.

colorless to red means that the non-covalented self-assembled samples were polymerized via the diacetinyl group. So, the polymerized red product has a reinforced form.

By comparing the physical properties (solubility and color change) of two compounds before and after polymerization, we also confirmed that the polymerization occurred. For example, the product after irradiation became insoluble in organic solvents such as DMSO, DMF, THF, $CHCl_3$, CH_3OH, and toluene. The insoluble product was isolated and its morphology was observed by SEM. The well-ordered helical structures of self-assembled **1** and **2** are still maintained after polymerization (Fig. S2). This finding is a rare example for the polymerized helical ribbon structure. However, the molecular weight of the polymerized helical ribbons could not be determined because of its insolubility in organic solvents such as DMSO, DMF, THF, $CHCl_3$, CH_3OH, and toluene.

2.3. A possible mechanism for the helical ribbon growth

SEM images indicate that the self-assembled **1** prepared by fast cooling possesses the helical ribbon structure with various pitches (10–24 μm) and with various ribbon widths (4–10 μm) in the initial stage (Fig. 4). Once again, both pitch and ribbon width values were changed during the process of helical ribbon growth. This finding strongly implies that the helical ribbon growth of alanine-based amphiphiles can be induced by two different pathways (Fig. 5). This is a rare example that examines the effect of the introduction of diacetylenic units on tubule growth that ultimately leads to the formation of the diacetylenic peptide-based amphiphiles.

We demonstrated the growth mechanism of the self-assemblies based on sugar and cholesterol derivatives in water or organic solvents. For example, the sugar-based lipid was induced by the mechanism illustrated in Figure 5a,[4a] whereas the cholesterol-based amphiphile was induced by that shown in Figure 5b.[5f] However, these self-assemblies **1** and **2** differ markedly from those observed with sugar- and cholesterol-based helical ribbons, which are formed by the mechanisms shown in Figure 5a or b. The helical ribbon growth process in these alanine-based amphiphiles is very rare, perhaps being influenced by formation conditions, cooling times, and driving forces related to hydrophobicity and hydrogen bond formation. However, the main factors that determine the mechanism of helical ribbon growth are not clear.

On the other hand, the self-assembled tube **1** prepared by slow cooling possesses a constant ribbon width (ca. 200 nm),

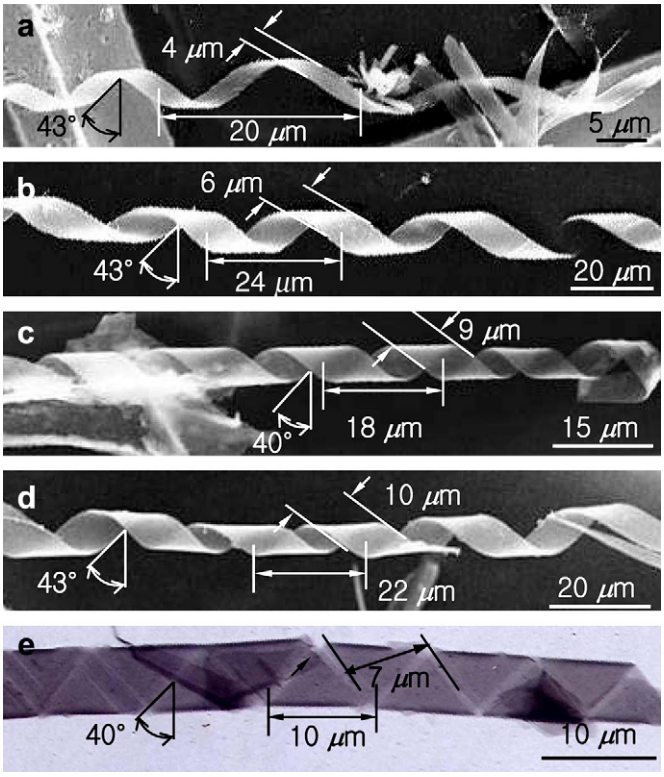

Figure 4. SEM or TEM images of the self-assembled helical ribbons with various pitches and various widths obtained from **1**.

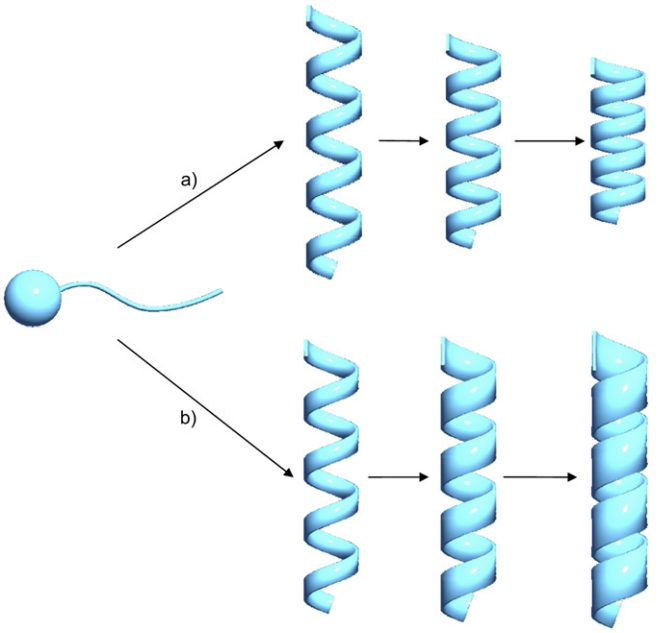

Figure 5. Representation of possible helical ribbon growth mechanisms of **1** and **2**: (a) the helical ribbon is formed by a change in the pitch length; (b) the helical ribbon is formed by growth in the width.

which indicates that the tubular structure is occurred by one process. However, it is not clear whether the tubular structure is induced by the mechanism shown in Figure 5a or b because the growth rate of the tubular structure is too fast for the intermediate to observe. Once again, the growth mechanism of the helical ribbon structure of self-assembled **1** prepared by fast cooling is quite different from that of the self-assembled **1** prepared by slow cooling.

2.4. CD measurement

CD spectroscopy is very useful for ascertaining the chiral molecular arrangement of self-assemblies.[3e,6h] For example, recently, Schnur and our group have studied on the chiral molecular architectures for self-assemblies of sugar or diacetylenic lipids by CD at different temperatures or solvents.[3e,6h]

In order to further test the effects of chirality, we have observed the CD and UV–vis spectra of the self-assembled **1**–**3** in water (see Fig. 6 and Fig. S3). In the CD spectra, $\lambda_{\theta=0}$ for the self-assembled **1** and **2** appeared at around 232 nm, which are originated from the amide group of alanine moiety by $n-\pi^*$ transition.[4a,15] On the other hand, the λ_{max} value in the UV absorption spectrum of **1** cannot be clearly observed due to the strong water peak at around 200 nm, however, the shoulder peak was observed at around 255 nm (Fig. S3). Thus it is not clear that CD spectra of the self-assembled **1**–**3** were induced by exciton coupling effect. However, the D-form (**1**) and the L-form (**2**) enantiomers showed the opposite CD signals as shown in Figure 6a and b, respectively. This result indicates that the helical ribbon structures of the two enantiomers have chiral molecular architectures with the opposite handedness, as would be expected. In addition, only weak CD signal of the self-assembled **1** at temperatures above

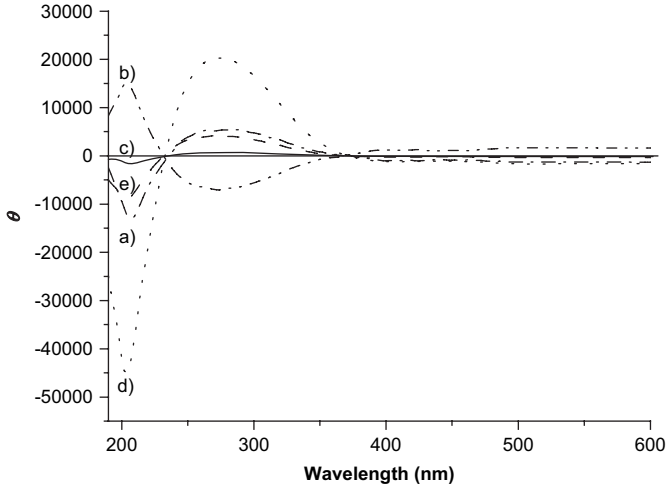

Figure 6. CD spectra of the self-assembled (a) **1** and (b) **2** prepared by fast cooling with 5.0 °C/min at 25 °C, (c) **1** at 70 °C, (d) **1** prepared by slow cooling with 0.5 °C/min, and (e) **3** prepared by fast cooling with 5.0 °C/min. The molar ellipticity [θ] is given in deg cm^2 dmol^{-1}.

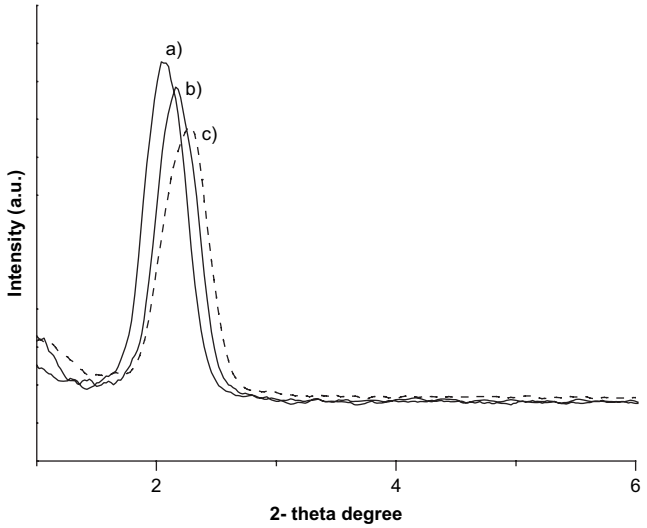

Figure 7. Powder XRD patterns of (a) self-assembled **1** prepared by fast cooling with 5.0 °C/min, (b) self-assembled **1** prepared by slow cooling with 0.5 °C/min, and (c) self-assembled **3** prepared by fast cooling with 5.0 °C/min.

a phase transition temperature (70 °C) was observed (Fig. 6c), which is probably composed of the monomers or small aggregates, such as micelles or vesicles. A strong CD signal reappeared when the self-assembled helical ribbon structure formed again after several hours.

We also measured CD spectrum of the self-assembled **1** prepared by slow and fast cooling to demonstrate different chiral molecular arrangements. The CD signal intensity of self-assembled **1** prepared by slow cooling (Fig. 6d) was much stronger than that by fast cooling. These findings indicate that the tubular form possesses the relatively well-ordered helical packing structure. On the other hand, the CD spectrum of the self-assembled **3** in aqueous solution showed a much weaker negative band (Fig. 6e) in comparison to **1** and **2**, suggesting that the self-assembled **3** forms disordered chiral packing structures.

2.5. Powder XRD measurement

We demonstrated the growth mechanism of the self-assemblies based on sugar and cholesterol derivatives in water or organic solvents. For example, the sugar-based lipid was induced by the mechanism illustrated in Figure 5a,[4a] whereas the cholesterol-based amphiphile was induced by that shown in Figure 5b.[5f] However, these self-assemblies **1** and **2** differ markedly from that observed with sugar- and cholesterol-based helical ribbons, which formed by the mechanisms in Figure 5a or b. The helical ribbon growth process in these alanine-based amphiphiles is very rare, perhaps being influenced by formation conditions, cooling times, and driving forces related to hydrophobicity and hydrogen bond formation. However, the main factors that determine the mechanism of helical ribbon growth are not clear.

Powder X-ray diffraction crystallography, a recently reported technique for ascertaining the molecular packing of self-assemblies,[4a,10,16] was used to clarify the self-assembling mechanism. The *d* values correspond to the distance for regularly arranged molecular packing. Particularly, if the self-assemblies form bilayered structures with a same orientation, the *d* value gives the relative distance for the interdigitated hydrophobic interaction between alkyl chain groups, which is related to the hydrophobic interaction. First, the molecular lengths of three amphiphiles were calculated using CPK space filling models and were determined to be highly similar. Secondly, X-ray diffraction patterns were measured. The *d*-spacing value of crystalline **1** from the self-assembled structures is shown in Figure 7. The small-angle diffraction patterns of helical ribbons **1** and **2** prepared by fast cooling appeared at 4.02 nm (Fig. 7a and Fig. S4), whereas the self-assembled tubes **1** and **2** prepared by slow cooling appeared at 4.29 nm. These values are smaller than twice the extended molecular length of **1** or **2** (2.80 nm using the CPK space filling model) but larger than the length of a single molecule. These results strongly suggest that the self-assembled **1** and **2** form a bilayered structure with a relative small region interdigitated by hydrophobic interaction as shown in Figure 7, due to the higher *d* value. Also, the hydrophobic interaction of the self-assembled tube was relatively weaker than that of the self-assembled helical ribbon.

On the other hand, the microcrystalline solid **3** (one molecular length: 2.84 nm) formed a bilayer structure with 3.69 nm, supporting the idea that **3** maintains a much larger interdigitated bilayer (Fig. 7c and Fig. S4) structure between the lipophilic regions than do those of **1** and **2**. The finding indicates that the relative strength of the hydrophobic interaction was dependent on the formation of the helical structure.

2.6. IR measurement

To confirm the morphological influences of the self-assembled **1** and **2** prepared at different pH conditions, we observed

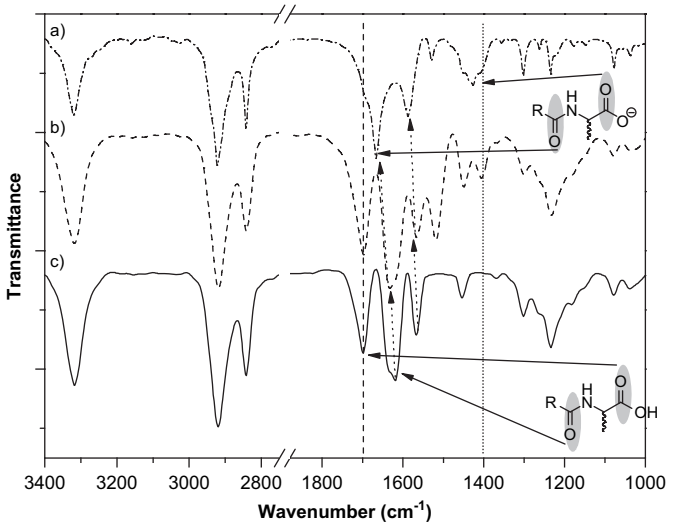

Figure 8. IR spectra of solution **1** at (a) pH=9, and of self-assembled **1** prepared at (b) pH=7 and (c) pH=4.

IR spectra of the self-assembled **1** formed at pH=4, 7, and 9, respectively (Fig. 8). Clearly, the helical ribbon formed at pH=7 with strong hydrogen bonding between the amide group and the highly organized, closely packed hydrocarbon chains produced sharper IR bands relative to the monomer species in aqueous solution at pH=9. Prominent differences were observed in a few regions. First, the helical ribbon **1** obtained at pH=7 displayed strong bands at 1701 and 1410 cm^{-1} for COOH and COO^- species, respectively. In contrast, the linear fiber **1** obtained at pH=4 showed only a single strong band at 1701 cm^{-1} for COOH. An alkaline solution of **1** (pH=9) shows a band for only the ionized COO^- species at 1410 cm^{-1}, which showed no solidified morphology. The results indicate that the intermolecular hydrogen bonding interactions between the COOH and COO^- species display a critical role to induce self-assembled superstructure of **1**. Secondly, amide function is characterized by three infrared absorption bands corresponding to the N–H stretch ($\nu_{NH} \approx 3322\ cm^{-1}$), the C=O stretch called the Amide I band ($\nu_{CO} \approx 1638\ cm^{-1}$) and a combination of the N–H deformation and the C–N stretch called the Amide II ($\delta_{NH}+\nu_{CN} \approx 1566\ cm^{-1}$). The intensities and wavenumbers of these bands are directly related to the hydrogen bond strength of the system. In the case of a transition from an associated amide to a free amide, the Amide I band is shifted to higher wavenumbers and the Amide II band to higher wavenumbers. Furthermore, the self-assembled **3** was confirmed by the intermolecular hydrogen bonding interaction between amide groups (Fig. S5).

3. Conclusions

The present study has demonstrated that D- and L-alanine-based amphiphiles possessing a diacetylene unit in the liphophilic region form right- and left-handed helical ribbon structures, respectively, depending on the stereochemical enantiomer. Thus, the self-assembled morphological helicity can be easily controlled by the alanine units. Interestingly, they form the tubular structure by slow cooling. However, the saturated long chain alanine-based amphiphile revealed the linear ribbon structure.

To the best of our knowledge, these results are a rare example of a systematic study on the influence of the alanine unit as a hydrophilic moiety and diacetylene unit in a hydrophobic portion on self-assembled morphologies. Based on the CD results, the self-assembled helical ribbon and nanotubular structure showed a relatively stronger intensity than that of the linear ribbon structure, indicating that the helical ribbon and nanotube formed relatively well-ordered chiral packing structures compared to the linear ribbon structure. Furthermore, in the XRD experiments, the relatively weak hydrophobic interactions of **1** and **2** formed with bilayered structures between the lipophilic groups led to the formation of the helical ribbon and nanotubular structures.

4. Experimental

4.1. General

^1H and ^{13}C NMR spectra were recorded with a DRX-500 (Bruker, 500 MHz) or an Avance-300 (Bruker, 300 MHz) NMR spectrometer. Preparative column chromatography was performed on silica gel. The chromatographic purity of the intermediates was monitored by thin-layer chromatography (Kiesel gel 60 F254, Merck). The compounds were visualized by spraying the plates with 5% sulfuric acid in methanol and then charring them on a hot plate. The molecular lengths were estimated by molecular mechanics calculations performed with the CONFLEX-MM2 force field as implemented in CAChe, version 4.1.1 (Fujitsu Co. Ltd., Japan). Circular dichroism (CD) spectra were measured on a JASCO J-715 spectrophotometer (cell diameter 1 mm).

4.1.1. TEM observations

The aqueous dispersions of the nanostructures (0.1 mg mL^{-1}) were dripped onto an amorphous carbon grid and excess water was blotted with filter paper. TEM was performed with a Carl-Zeiss LEO912 instrument operated at 50 keV. Images were recorded on an imaging plate (Fuji Photo Film Co. Ltd. FDL5000 system) with 20-eV energy windows at 3000–250,000× and were digitally enlarged.

4.1.2. FTIR measurements

The FTIR spectra of the self-assembled nanostructures were measured with a Fourier transform IR spectrometer (JASCO FT-620) operated at 4 cm^{-1} resolution with an unpolarized beam, attenuated total reflection (ATR) accessory system (Diamond MIRacle, horizontal ATR accessory with a diamond crystal prism, PIKE Technologies, USA) and a mercury cadmium telluride (MCT) detector. Several drops of the aqueous dispersions of the self-assembly were dripped onto the prism and dried under nitrogen stream prior to measurement.

4.1.3. XRD measurements

The XRD of a freeze-dried sample was measured with a Rigakudiffractometer (Type 4037) using graded *d*-space elliptical side-by-side multilayer optics, monochromated Cu Kα radiation (40 kV, 30 mA) and an imaging plate (R-Axis IV). The typical exposure time was 10 min with an 150-mm camera length. Freeze-dried samples from **1** to **3** were vacuum dried to constant weight and then put into capillary tubes, without being powdered.

4.1.4. CD measurements

Circular dichroism (CD) studies were performed on a JASCO J-715 spectropolarimeter operating between 190 and 500 nm. The samples (5.0×10^{-3} M) were placed in water-jacketed quartz cells with path lengths of 0.1 mm. Temperature control was provided by a water circulator, which provided a thermal stability of about 0.2 °C. The spectrometer was calibrated with ammonium-D-camphorsulfonate ($[\theta]_{291}=7910$ deg cm^2 dmol^{-1}) and D-pantonyllactone ($[\theta]_{219}=-16{,}140$ in water, $[\theta]_{223}=-12{,}420$ in methanol).

*4.1.5. pH adjustment of the self-assembled **1–3***

Aqueous dispersion (10 mL) was prepared by adding degassed distilled water to a weighted powder of **1–3** and succeeding sonication at 25 °C. The pH values of aqueous dispersions were then adjusted with 0.1 M NaOH or 0.1 M HCl solution. During the heating and irradiation processes, the sample flask was wrapped with Al foil to prevent the polymerization.

*4.1.6. Compound **7***

Thionyl chloride (12.5 mL) was added dropwise to stirred and cooled (−10 °C) ethanol (50 mL), followed by the addition of D-alanine (4.46 g, 50 mmol). The temperature of the solution was increased and maintained at 40 °C for 4 h. The solvent was removed and crystallization from methanol/ethyl ether yielded 4.65 g (86%). Mp 76–78 °C.[17] ^{1}H NMR (300 MHz, DMSO-d_6, 25 °C): δ 8.66 (s, 3H, NH_3), 4.17 (q, 1H, J=7.2 Hz), 4.00 (q, 2H, J=7.2 Hz), 1.40 (d, 3H, J=7 Hz), 1.22 (t, 3H, J=7.2 Hz).

*4.1.7. Compound **8***

Compound **8** was prepared by a method similar to that used for **7** in 78% yield. Mp 76–78 °C. ^{1}H NMR (300 MHz, DMSO-d_6, 25 °C): δ 8.66 (s, 3H, NH_3), 4.17 (q, 1H, J=7.2 Hz), 4.00 (q, 2H, J=7.2 Hz), 1.40 (d, 3H, J=7 Hz), 1.22 (t, 3H, J=7.2 Hz).

*4.1.8. Compound **4***

Compound **6** (100 mg, 0.4 mmol) was dissolved in ethyl acetate (4 mL), and DCC (105.6 mg, 0.51 mmol) and HOBt (69.2 mg, 0.51 mmol) were added after cooling to 0 °C. The mixture was stirred for 30 min whereupon compound **7** (55 mg, 0.36 mmol) and triethylamine (40 mg, 0.4 mmol) were added. The reaction mixture was stirred at room temperature overnight. The insoluble material was filtered off and the solution was washed successively with saturated $NaHCO_3$, saturated $NaHSO_4$, and saturated $NaHCO_3$. After drying with $MgSO_4$ the solvents were removed under reduced pressure. This crude product was purified by column chromatography (ethyl acetate/hexane, 1/2) to give the product (70%). Mp 81.3–82.0 °C. ^{1}H NMR (300 MHz, $CDCl_3$, 25 °C): δ 5.82 (s, 1H, NH), 4.58 (q, 1H, J=6 Hz), 4.17 (q, 2H, J=7.2 Hz), 2.18 (t, 2H, J=6.9 Hz), 2.05 (m, 4H), 1.54–1.30 (m, 22H), 0.91 (t, 3H, J=7.2 Hz); ^{13}C NMR (75 MHz, $CDCl_3$, 25 °C): δ 176, 174, 71, 65, 60, 45, 32, 31–29, 21, 17, 15; IR (KBr): $\tilde{\nu}$=3322, 2957, 2917, 2849, 1742, 1648, 1537, 1472, 1421, 1030, 951; MS (FAB) *m/z* 362 $(M+H)^+$. Anal. Calcd for $C_{23}H_{45}NO_3$: C, 73.09; H, 9.76; N, 3.87. Found C, 73.15; H, 10.01; N, 3.64.

*4.1.9. Compound **5***

Compound **5** was prepared by a method similar to that used for **4** in 75% yield. Mp 80.8–82.0 °C. ^{1}H NMR (300 MHz, $CDCl_3$, 25 °C): δ 5.82 (s, 1H, NH), 4.58 (q, 1H, J=6 Hz), 4.17 (q, 2H, J=7.2 Hz), 2.18 (t, 2H, J=6.9 Hz), 2.05 (m, 4H), 1.54–1.30 (m, 22H), 0.91 (t, 3H, J=7.2 Hz); ^{13}C NMR (75 MHz, $CDCl_3$, 25 °C): δ 176, 174, 71, 65, 60, 45, 32, 31–29, 21, 17, 15; IR (KBr): $\tilde{\nu}$=3322, 2957, 2917, 2849, 1742, 1648, 1537, 1472, 1421, 1030, 951; MS (FAB) *m/z* 362 $(M+H)^+$; Anal. Calcd for $C_{23}H_{45}NO_3$: C, 73.09; H, 9.76; N, 3.87. Found C, 73.01; H, 9.57; N, 3.63.

*4.1.10. Compound **1***

Compound **4** (120 mg, 0.33 mmol) was dissolved in methanol (5 mL) and 1 M NaOH (1 mL, 1 mmol) was added. The mixture was stirred at room temperature for 4 h and 1 M HCl (2.5 mL, 2.5 mmol) was then added. The methanol was removed under reduced pressure and the solution thus obtained was cooled in an ice bath and acidified with 1 M HCl (3 mL) with vigorous stirring and extracted with ethyl acetate (50 mL). The organic layer was dried over $MgSO_4$. Removal of the organic solvent in vacuo afforded a white solid. This crude product was purified by column chromatography (ethanol/hexane) to give the product (95%). Mp 92.0–93.1 °C. ^{1}H NMR (300 MHz, $CDCl_3$, 25 °C): δ 8.01 (s, 1H), 4.45 (q, 1H, J=6 Hz), 2.24 (t, 2H, J=6.9 Hz), 2.10 (m, 4 H), 1.58–1.35 (m, 19H), 0.93 (t, 3H, J=7.2 Hz); ^{13}C NMR (75 MHz, $CDCl_3$, 25 °C): δ 175, 174, 74, 68, 31, 31–29, 20, 16, 15; IR (KBr): $\tilde{\nu}$=3315, 2915, 2839, 1696, 1633, 1565, 1518, 1449, 1405, 1300, 1231, 1078, 910, 705, 631, 565, 533; MS (FAB) *m/z* 334 $(M+H)^+$. Anal. Calcd for $C_{20}H_{31}NO_3$: C, 72.04; H, 9.37; N, 4.20. Found C, 72.51; H, 9.51; N, 4.41.

*4.1.11. Compound **2***

Compound **2** was prepared by a method similar to that used for **1** in 92% yield. Mp 91.5–93.5 °C. ^{1}H NMR (300 MHz, $CDCl_3$, 25 °C): δ 8.01 (s, 1H), 4.45 (q, 1H, J=6 Hz), 2.24 (t, 2H, J=6.9 Hz), 2.10 (m, 4H), 1.58–1.35 (m, 19H), 0.93 (t, 3H, J=7.2 Hz); ^{13}C NMR (75 MHz, $CDCl_3$, 25 °C): δ 175, 174, 74, 68, 31, 31–29, 20, 16, 15; IR (KBr): $\tilde{\nu}$=3315, 2915, 2839, 1696, 1633, 1565, 1518, 1449, 1405, 1300, 1231, 1078, 910, 705, 631, 565, 533; MS (FAB) *m/z* 334 $(M+H)^+$. Anal.

Calcd for $C_{20}H_{31}NO_3$: C, 72.04; H, 9.37; N, 4.20. Found C, 72.55; H, 9.53; N, 4.31.

4.1.12. Compound **11**

To a solution of **7** (1 g, 6.44 mmol) in dry THF (20 mL) at 56 °C under N_2 was added TEA (4 g, 39.61 mmol). The reaction mixture was stirred at 56 °C for 10 min. To the reaction mixture were added stearoyl chloride and **8** (1.5 g, 4.95 mmol). After 1 h, the precipitate was removed by filtration. Then the solvent was removed by rotary evaporation to produce a yellow solid. This crude product was purified by column chromatography (ethyl acetate/hexane, 1/3) to give the product **9** (1.41 g, 78%). ^{1}H NMR (300 MHz, $CDCl_3$, 25 °C): δ 6.04 (s, 1H, NH), 4.60 (q, 1H, J=6 Hz), 4.21 (q, 2H, J=7.2 Hz), 2.22 (t, 2H, J=7.2 Hz), 1.67 (m, 3H), 1.41–1.27 (m, 33H), 0.89 (t, 3H, J=6.9 Hz); ^{13}C NMR (75 MHz, $CDCl_3$, 25 °C): δ 173, 172, 61, 47, 36, 31–29, 25, 22, 18, 14; IR (KBr): $\tilde{\nu}$=3322, 2957, 2915, 2849, 1742, 1648, 1537, 1472, 1415, 1381, 1201, 1165, 1030, 717, 668; MS (FAB) *m/z* 384 $(M+H)^+$. Anal. Calcd for $C_{23}H_{45}NO_3$: C, 72.01; H, 11.82; N, 3.65. Found C, 71.84; H, 12.01; N, 3.58.

4.1.13. Compound **3**

Compound **3** was prepared by a method similar to that used for **1** in 43% yield. Mp 96.0–97.2 °C. ^{1}H NMR (300 MHz, $CDCl_3$, 25 °C): δ 8.51 (s, 1H), 4.39 (q, 1H, J=6.9 Hz), 3.3 (s, 1H), 2.24 (t, 2H, J=7.5 Hz), 1.63 (m, 3H), 1.3 (m), 0.92 (t, 3H, J=6.9 Hz); ^{13}C NMR (75 MHz, $CDCl_3$, 25 °C): δ 174.7, 174.6, 35, 31, 29–27, 25, 22, 16, 13; IR (KBr): $\tilde{\nu}$=3316, 2905, 2848, 1707, 1645, 1541, 1467, 1415, 1247, 924, 716; MS (FAB) *m/z* 356 $(M+H)^+$. Anal. Calcd for $C_{21}H_{41}NO_3$: C, 70.94; H, 11.62; N, 3.94. Found C, 70.01; H, 11.2; N, 3.65.

Acknowledgements

This work was supported by KRF (KRF-2005-070-C00068) and KOSEF (R01-2005-000-10229-0 and M20702000050-07B-0200-05000). In addition, this work is partially supported by Korea Ministry of Environment as 'The Eco-technopia 21 Project'.

Supplementary data

It includes synthetic routes, SEM images, molecular packing structure, and IR spectrum of self-assembled **1** and **2**. Supplementary data associated with this article can be found in the online version, at doi:10.1016/j.tet.2007.11.062.

References and notes

1. Stinson, S. C. *Chem. Eng. News* **2000**, *78*, 55.
2. Kamien, R. D.; Selinger, J. V. *J. Phys.: Condens. Matter* **2001**, *13*, R1.
3. (a) Jung, J. H.; Shinkai, S.; Shimizu, T. *Chem. Rec.* **2003**, *3*, 212; (b) Jung, J. H.; Shinkai, S. *Top. Curr. Chem.* **2004**, *58*, 223; (c) Shimizu, T.; Masuda, M.; Minamikawa, H. *Chem. Rev.* **2005**, *105*, 1401; (d) John, G.; Mason, M.; Ajayan, P. M.; Dordick, J. S. *J. Am. Chem. Soc.* **2004**, *126*, 15012; (e) Jung, J. H.; John, G.; Yoshida, K.; Shimizu, T. *J. Am. Chem. Soc.* **2002**, *124*, 10674.
4. (a) Jung, J. H.; John, G.; Yoshida, K.; Shimizu, T. *J. Am. Chem. Soc.* **2002**, *124*, 10674; (b) John, G.; Jung, J. H.; Minamikawa, H.; Yoshida, K.; Shimizu, T. *Chem.—Eur. J.* **2002**, *8*, 5494; (c) John, G.; Jung, J. H.; Masuda, M.; Shimizu, T. *Langmuir* **2004**, *20*, 2060.
5. (a) Ono, Y.; Kanekiyo, K.; Inoue, K.; Hojo, J.; Shinkai, S. *Chem. Lett.* **1999**, 23; (b) Jung, J. H.; Ono, Y.; Shinkai, S. *J. Chem. Soc., Perkin Trans. 2* **1999**, 1289; (c) Jung, J. H.; Ono, Y.; Shinkai, S. *Langmuir* **2000**, *16*, 1643; (d) Jung, J. H.; Ono, Y.; Shinkai, S. *Angew. Chem., Int. Ed.* **2000**, *39*, 1862; (e) Jung, J. H.; Ono, Y.; Sakurai, K.; Sano, M.; Shinkai, S. *J. Am. Chem. Soc.* **2000**, *122*, 8648; (f) Jung, J. H.; Kobayashi, H.; Masuda, M.; Shimizu, T.; Shinkai, S. *J. Am. Chem. Soc.* **2001**, *123*, 8785.
6. (a) Fuhrhop, J. H.; Spiroski, D.; Boettcher, C. *J. Am. Chem. Soc.* **1993**, *115*, 1600; (b) Shimizu, T.; Hato, M. *Biochim. Biophys. Acta* **1993**, *1147*, 50; (c) Shimizu, T.; Kogiso, M.; Masuda, M. *Nature* **1996**, *383*, 487; (d) Kogiso, M.; Ohnishi, S.; Yase, K.; Masuda, M.; Shimizu, T. *Langmuir* **1998**, *14*, 4978; (e) Kogiso, M.; Okada, Y.; Yase, T.; Shimizu, T. *Biochim. Biophys. Acta* **2000**, *1475*, 346; (f) Kogiso, M.; Zhou, Y.; Shimizu, T. *Adv. Mater.* **2007**, *19*, 242; (g) Spector, M. S.; Easwaran, K. R. K.; Jyothi, G.; Selinger, J. V.; Singh, A.; Schnur, J. M. *Proc. Natl. Acad. Sci. U.S.A.* **1996**, *93*, 12943; (h) Schnur, J. M.; Ratna, B. R.; Selinger, J. V.; Singh, A.; Jyothi, G.; Easwaran, K. R. K. *Science* **1994**, *264*, 945; (i) Spector, M. S.; Selinger, J. V.; Singh, A.; Rodriguez, J. M.; Price, R. R.; Schnur, J. M. *Langmuir* **1998**, *14*, 3493.
7. (a) Kim, J.-M.; Ji, E.-K.; Woo, S. M.; Lee, H.; Ahn, D. J. *Adv. Mater.* **2003**, *15*, 1118; (b) Ahn, D. J.; Chae, E.-H.; Lee, G. S.; Shim, H.-Y.; Chang, T.-E.; Ahn, K.-D.; Kim, J.-M. *J. Am. Chem. Soc.* **2003**, *125*, 8976; (c) Kim, J.-M.; Lee, Y. B.; Yang, D. H.; Lee, J.-S.; Lee, G. S.; Ahn, D. J. *J. Am. Chem. Soc.* **2005**, *127*, 17580; (d) Kim, J.-M.; Lee, J.-S.; Choi, H.; Sohn, D.; Ahn, D. J. *Macromolecules* **2005**, *38*, 9366.
8. Song, J.; Cheng, Q.; Kopta, S.; Stevens, R. C. *J. Am. Chem. Soc.* **2001**, *123*, 3205.
9. (a) Nakashima, N.; Asakuma, S.; Kim, J. M.; Kunitake, T. *Chem. Lett.* **1984**, 1709; (b) Yamada, K.; Ihara, H.; Ide, T.; Fukumoto, T.; Hiyayama, C. *Chem. Lett.* **1984**, 1713; (c) Nakashima, N.; Asakuma, S.; Kunitake, T. *J. Am. Chem. Soc.* **1985**, *107*, 509; (d) Shoen, P. E.; Yager, P. *Mol. Cryst. Liq. Cryst.* **1984**, *106*, 371.
10. Sumiyoshi, T.; Nishimura, K.; Nakano, M.; Handa, T.; Miwa, Y.; Tomioka, K. *J. Am. Chem. Soc.* **2003**, *125*, 12137.
11. (a) Shimizu, T.; Mori, M.; Minamikawa, H.; Hato, M. *Chem. Lett.* **1989**, 1341; (b) Shimizu, T.; Hato, M. *Thin Solid Films* **1989**, *180*, 179; (c) Shimizu, T.; Mori, M.; Minamikawa, H.; Hato, M. *J. Chem. Soc., Chem. Commun.* **1990**, 183; (d) Fuhrhop, J. H.; Blumtritt, P.; Lehmann, C.; Lugar, P. *J. Am. Chem. Soc.* **1991**, *113*, 7437; (e) Frankel, D. A.; O'Brien, D. F. *J. Am. Chem. Soc.* **1991**, *113*, 7436.
12. (a) Djalali, R. D.; Chen, Y.-f.; Matsui, H. *J. Am. Chem. Soc.* **2003**, *125*, 5873; (b) Porrata, P.; Goun, E.; Matsui, H. *Chem. Mater.* **2002**, *14*, 4378.
13. Brizaed, A.; Aime, C.; Labort, T.; Huc, I.; Berthier, D.; Artzner, F.; Desbat, B.; Oda, R. *J. Am. Chem. Soc.* **2007**, *129*, 3754.
14. (a) Chung, D. S.; Benedek, G. B.; Konikoff, F. M.; Donovan, J. M. *Proc. Natl. Acad. Sci. U.S.A.* **1993**, *90*, 11341; (b) Matsui, H.; Douberly, G. E., Jr. *Langmuir* **2001**, *17*, 7918; (c) Löwik, D. W.; Garacia-Hartjes, J.; Meiher, J. T.; van Hest, J. C. M. *Langmuir* **2005**, *21*, 524; (d) Brizard, A.; Ahmad, R. K.; Oda, R. *Chem. Commun.* **2007**, 2275.
15. Sreerama, N.; Woody, R. W. Circular Dichroism of Peptides and Proteins. In *Circular Dichroism: Principles and Applications*, 2nd ed.; Berova, N., Nakanishi, K., Woody, R. W., Eds.; John Wiley & Sons: New York, NY, 2000; pp 601–620.
16. Masuda, M.; Shimizu, T. *Langmuir* **2004**, *20*, 5969.
17. Jakusch, T.; Dörnyei, A.; Correia, I.; Rodrigues, L. M.; Tóth, G. K.; Kiss, T.; Pessoa, J. C.; Marcão, S. *Eur. J. Inorg. Chem.* **2003**, 2113.